Carbon Nanotube Coated Paper Sensor for Damage Diagnosis

Beomseok Kim,*,† Yijiang Lu,† Taemin Kim,‡ Jin-Woo Han,§ M. Meyyappan, and Jing Li

†ELORET Corportaion, ‡SGT, Inc., and §University Space Research Association (USRA), NASA Ames Research Center, Moffett Field, California 94035, United States

ABSTRACT A carbon nanotube coated paper sensor has been developed for the detection of damages in structural components. Electrical resistance tomography is used to measure changes in electrical potential at various locations induced by applying a small electrical current to the sample. The spatial locations and magnitudes of multiple damages are predicted accurately with a sensitivity of 73 ppm in sensing area. The detection limit of the sensor is estimated to be 29 ppm in sensing area, which is at least 30 times better in sensitivity than previous results (0.1−0.65%) in the literature.

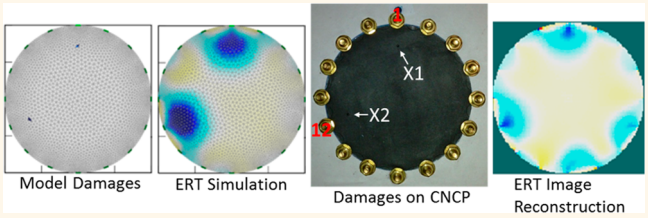

KEYWORDS: carbon nanotube · paper sensor · structural diagnosis · electrical resistance tomography

Catastrophic structural failures cause significant physical and personal losses, and thus, development of nondestructive real-time health monitoring of structural systems has been receiving much attention.[1] The need exists in several fields including civil aviation, spacecraft, military vehicles, automobiles and other transportation systems, pressure vessels, and many others. A variety of discrete sensors such as strain gauges or piezoelectric transducers have been used for detecting regions of damage in real-time. However, many of the methods, including those reported in the literature and commercial products, are prone to be inherently complex or incur a weight penalty due to the weight of discrete sensors and wiring requirements.[2] Electrical resistance tomography (ERT) has been introduced to overcome these disadvantages.[3] ERT uses the material as a sensor without any additional discrete sensor components to diagnose damages on the material surface. Changes in electrical potential at various locations are measured by applying small electrical currents to the material. The damaged spatial location and its magnitude are predicted by solving the inverse problem based on the measurements. For an object with unknown electrical properties, reconstruction of an image requires determination of the internal conductivity profile of the object from a finite number of boundary measurements.

Advances in nanomaterials have enabled lightweight and highly sensitive devices for damage detection in recent years. Carbon nanotubes (CNTs) have been investigated for enhancing structural performance of composite materials with significantly reduced weight and enhanced electrical conductivity, and these developments could be used for damage sensing and inspection,[4−11] as has been done previously with other carbon materials.[12,13] ERT has been applied for spatial characterization of the conductivity of carbon nanotube composite thin films and several groups have reported their initial observations using ERT and its variations.[1,4−6] For example, two-dimensional damage maps have been generated using electrical impedance tomography to establish the extent of damage at a given location under impact loading.[1] Discontinuities as small as 0.1% of the area under inspection have been detected using carbon fiber reinforced polymer plates.[4] Mapping the response of the film under investigation to varying pH of the environment besides imaging the structural defects has also been demonstrated.[5,6] These developments are encouraging, however, predictability and sensitivity toward small damages still need to be improved. In this work, we focus on key parameters to improve damage diagnosis, particularly the sensing material and implementing efficient image reconstruction of the damaged location. We use carbon nanotube coated paper

* Address correspondence to beomseok.kim@nasa.gov.

Received for review April 22, 2014 and accepted November 17, 2014.

Published online November 17, 2014
10.1021/nn5037653

Figure 1. (a) A thin plastic tape with carbon nanotube coated paper to enhance physical durability, front (left) and back (right) of the CNCP (d = 7 cm). (b) CNCP fixed with 16 electrodes, located around the CNCP boundary. Numbering of the electrodes is clockwise starting from top (1 in red colored). The closest distance between two adjacent electrodes is 0.6 mm. Two intentional damages (X1 and X2) are located at 1 cm from the CNCP periphery near electrode 1 and 12.

(CNCP) as sensing material here and show an order of magnitude higher sensitively in damage detection than previous literature results. The relative thin size of the paper combined with the superior conductive properties of CNTs allows sensitive detection of damages as shown here. Paper as a substrate has received much attention in recent years for humidity and gas/vapor sensors,[14−16] energy storage devices[17] and many other applications. Adding a highly conductive material such as single-walled carbon nanotubes (SWCNTs) either as a thin film or making a paper−CNT composite increases the functionality to attractive sensing opportunities, which is exploited here.[15,18]

RESULTS AND DISCUSSION

The carbon nanotube-coated paper has several advantages over other materials such as conductive glass carbon panel or carbon-fiber-reinforced polymer (CFRP). The CNCP is conductive cellulose, which is easily modifiable, thin, flexible, and works under extremely low temperatures including cryogenic conditions. However, it is prone to be damaged by external forces due to the nature of paper and hence, it is well suited for damage sensing.

The CNCP was prepared by deposition of dispersed single-walled carbon nanotubes[17−19] onto a 7 cm filter paper (Figure 1a). Details are provided under Materials and Methods. Electrical resistance tomography was performed to measure changes in conductivity within the CNCP due to intentionally induced damage. In addition to detection of damage, the capability to detect multiple damages was tested as it relates to spatial sensing capability of the CNCP. Background information on ERT, solution of the inversion problem and related details[20−23] are provided in Supporting Information. Two intentional holes to simulate multiple damages were introduced to the CNCP with two different size needles, whose diameters were measured by a digital vernier caliper. The damages X1 and X2 (0.6 and 1.1 mm) were located 1 cm away from electrodes 1 and 12, respectively (Figure 1b). The injection current to the CNCP samples was limited by the potential measurement system to 21 V. The ERT experiments were done under various injection currents to optimize the experimental conditions. The highest injection current (20 mA) on sample A showed the best result because the high current enables to see a big potential difference by the damages (Figure 2d).

The reconstructed images in Figure 2d show two damages clearly near electrodes 1 (top) and 12 (left below), which can be shown simultaneously. However, ghost images (noise) are also seen around electrodes 6 and 8 probably due to measurement artifacts. As injection current decreases, the damages in the reconstructed images begin to fade. Finally, the damages cannot be seen at the lowest injection current (Figure 2a).

Figure 3 shows quantitative information on surface conductivity change *vs* total damaged area on sample A discussed above. The conductivity change is quantifiable by standard deviation (σ) of the z component, surface conductivity of the reconstructed images in 3D representation. In addition, the standard deviation is statistically useful over mean of the surface conductivity because the damage response shows only less conductivity with negative direction in 3D representation.[1] For evaluation and comparison of reconstructed 2D images, the 3D representation and quantification of the reconstructed conductivity map are critical because 3D images include the magnitude information on damages. The key parameters such as hyperparameter and induced electric current greatly influence the constructed results (see Supporting Information). Thus, the reconstructed images under different parameter sets cannot be compared; however, if all the parameters are fixed and controllable, we can compare the results relatively. On the basis of the simulation results of related parameters described in Supporting Information, even the smallest damage at 0.4 mm could impact on the entire sensor surface conductivity.

The higher current enables to see the slope and linearity increase (R^2) clearly as the total damaged area increases. The slope increase from 0.4×10^{-3} to 2.4×10^{-3}, which is intercepted at 0, is proportional to the current increase. At the smallest 0.28 mm^2 damage, the

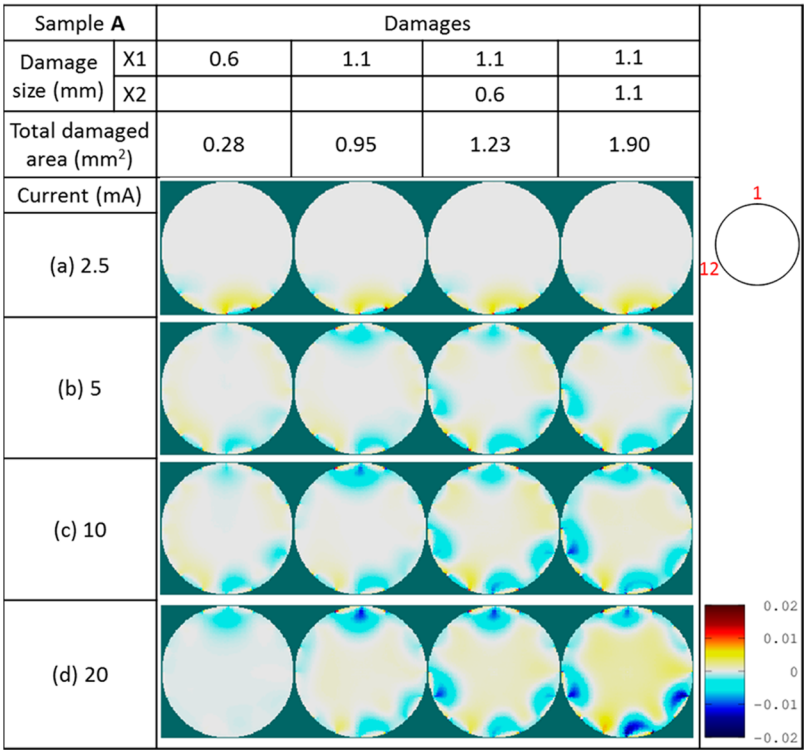

Figure 2. Conductivity map of damage locations within the same sample A, under various injection currents from 2.5 to 20 mA and total damaged area from 0.28 to 1.9 mm^2. Two damages, X1 and X2, are located at 1 cm from electrode 1 and 12. (a) Reconstructed images do not show any damage at 2.5 mA. However, reconstructed images show damages, X1 and X2, (b) at 5 mA, (c) at 10 mA, and (d) at 20 mA. The highest response was obtained (d) at 20 mA at 1.9 mm^2 damage, which is used to normalize the color legend of all images in relative and arbitrary units.

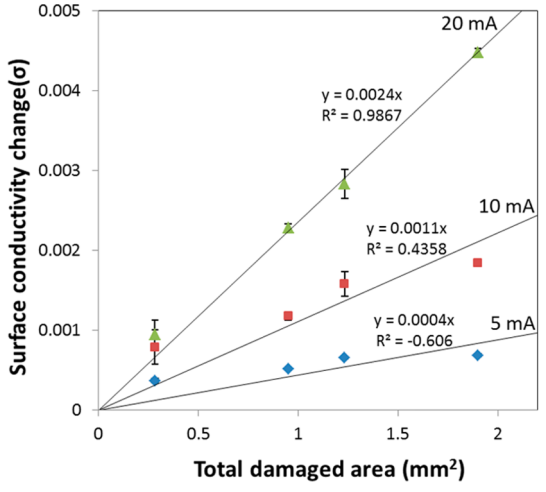

Figure 3. Surface conductivity changes (σ) of sample A under various currents based on Figure 2. The higher injection current, 20 mA, shows more linearity on surface conductivity change (σ) toward total damaged area. The sample at 2.5 mA is not included because it shows out of chart range. Measurement error (2σ) depicted within each error bar.

relative standard deviation (RSD) in three consecutive measurements is 20% due to the background noise. This number reduces to 1% for the largest two damages, 1.9 mm^2 because the larger damages provide stronger signal over the background noise.

Damage detection capability was tested with other samples with higher base resistance values (B and C) in a similar way as described in Supporting Information. However, they failed to show damages clearly from the ERT as shown in Supporting Information Figure S2. Therefore, we conclude that lower resistance (<1 MΩ) over the sample is required to inject higher current in order to obtain clear response from the ERT technique. The sensor response is clear with accurate spatial locations and magnitude from the 0.6 mm size damage on the CNCP in sample A. The experimental detection limit from this result is 73 ppm or 73 $\times$ 10^{-6} in area.

Repeat tests with different damage sizes from 1 to 3 mm by 1 mm size increase were done with sample A′ for the purpose of calibration and derivation of detection limit (Figure 4). The overall resistance of the duplicated sample A′ is slightly lower than sample A. The damages were made with corresponding size metal drills. Larger size damages (1−3 mm) also show accurate spatial locations and increased magnitude as the damage size is increased (see Figure 4b). In Figure 4, the noise level is relatively small and the damaged location is pronounced. About the locations of detected damages, we have simulated and quantified these in Table S4 in Supporting Information. In summary, the size of the response area is orders bigger than the size of the damage. Thus, the peak coordinates are always within the response even if the

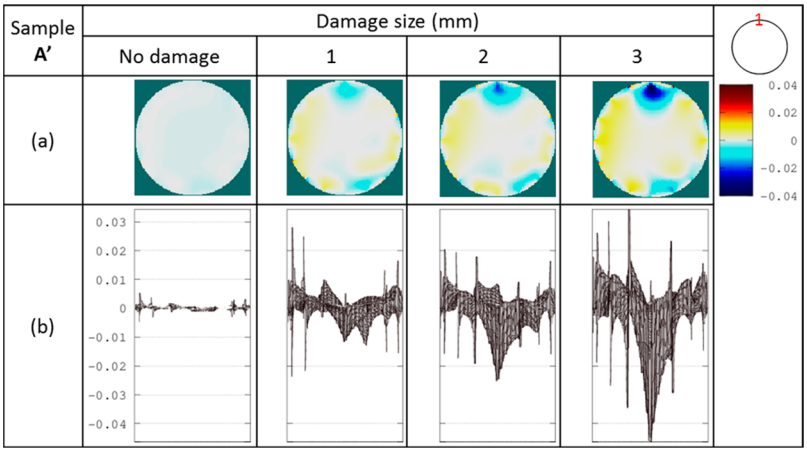

Figure 4. Conductivity map of damage locations, sized from 0 to 3 mm, (a) sample A′ at 20 mA current injection, and (b) 3D side view of images directionally from electrode 9 to electrode 1. Color legend of all images is in relative and arbitrary units.

TABLE 1. Surface Conductivity Change for Different Damage Sizes from 1 to 3 mm, in Standard Deviation of the CNCP Surface Obtained from Figure 4,[a]

	surface conductivity change (σ) of the CNCP surface at three measurements				
damage size (mm)	1	2	3	$\bar{\sigma}$	$\sigma\bar{\sigma}$
0	0.86×10^{-3}	0.43×10^{-3}	0.12×10^{-3}	0.82×10^{-3}	0.37×10^{-3}
1	2.73×10^{-3}	2.66×10^{-3}	2.65×10^{-3}	2.68×10^{-3}	0.04×10^{-3}
2	5.77×10^{-3}	5.86×10^{-3}	5.82×10^{-3}	5.81×10^{-3}	0.04×10^{-3}
3	8.91×10^{-3}	8.81×10^{-3}	8.79×10^{-3}	8.84×10^{-3}	0.07×10^{-3}

[a] The results were measured and calculated 3 times and averaged.

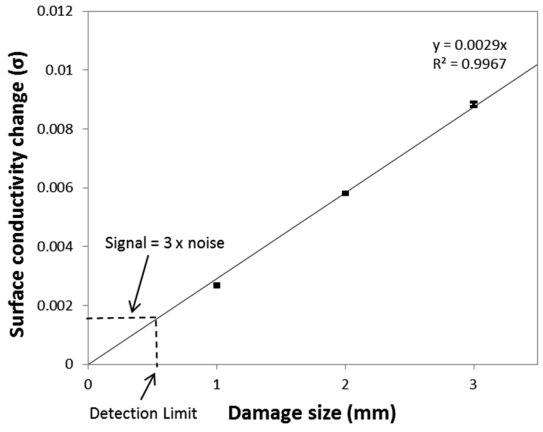

Figure 5. Calibration curve, data obtained from Table 1, using averaged standard deviation (σ). The error bars show measurement error (2σ).

distance errors can be up to 20 times of the damage diameter. Table 1 shows the calculated σ of the CNCP surface conductivity obtained from Figure 4. Figure 5 depicts the damage size in mm *versus* surface conductivity change in σ.

The lowest detectable damage was limited by the noise from the experimental setup. The standard deviation of averaged sensor noise from undamaged CNCP surface is 0.37×10^{-3} (see Table 1). According to the IUPAC definition,[24] when the signal-to-noise ratio equals 3, the signal is considered to be a true signal. Therefore, the detection limit can be extrapolated from the linear calibration curve (Figure 5).

$$\text{detection limit (mm)} = \frac{3\sigma}{\text{slope}}$$

With the above equation, the damage detection limit is calculated to be 0.38 mm damage in 7 cm diameter CNCP sensor at the average noise level. This value is equivalent to 29 ppm or 29×10^{-6} in area. Indeed, this derived detection limit is lower than the smallest tested size of of 0.6 mm here.

The superior performance of the CNCP sensor can be attributed to the relative thin size of the device enabled by the cellulose paper and high conductivity of the SWCNTs. The results for samples of varying resistance values clearly indicate the need to have a low resistance medium for sensitive detection. Our observation with thick panel samples is similar to previous findings including the detection limit to be much lower with thicker panels. Though we could not vary the thickness of the paper substrate itself here, we tested electrically conductive Garolite glass carbon (Item# 2235K4, McMaster-Carr) with a sample diameter 12.7 cm and thickness of 3.2 mm. The sensor response was clear with accurate spatial locations and magnitude from a 3 mm diameter damage (quite larger than the 0.6 mm minimum size tested here). The experimental detection

limit from this test was 560 ppm or 5.6×10^{-4} in area. Thus, we conclude that the observed difference in detection limit is mainly due to the increased thickness of the above sample compared to the filter paper with a thickness less than 0.2 mm including the plastic thin film. A thicker sample has more possible electron conductive paths in its three-dimensional sample volume. As the sample gets thinner approaching negligible dimensions in that direction, electron motion will be increasingly restricted to two dimensions. The reduction of conducting paths in thinner samples then increases the damage discontinuities relatively. Thus, thinner, highly conductive, and low background noise sample such as a nanomaterial thin films including SWCNTs and graphene would be the best sensing material for damage diagnosis using ERT.

Finally, we compare the damage detection performance of our CNCP sensor with previously published results. Ross *et al.*[2] tested CHO-SEAL 1285, a conductive elastomer consisting of silver-plated aluminum particles in a silicone binder, sized 20.3 cm × 20.3 cm × 25.4 mm. They used a neural network-based damage diagnosis model to solve the inverse problem. The damage diameter was 18.5 mm and the detection limit was 0.65% in area. Baltopoulos *et al.* used CFRP, sized 10 cm × 10 cm × 1.5 mm, with a damage diameter of 3 mm and with the aid of EIDORS packages, could detect discontinuities as small as 0.1% of the inspected area.[4] Our results here show an order of magnitude better sensitivity compared to these earlier reports.

CONCLUSIONS

Carbon nanotube coated paper (CNCP) has been used as a sensor material to identify spatial structural damages. The CNCP has several advantages over other materials such as easy fabrication, very small thickness, flexibility and low temperature operation down to cryogenic temperatures. This highly conductive paper has been made from aqueous carbon nanotube ink with a surfactant. Boundary potentials are collected by a circular 16-electrode array around the CNCP and resistivity images are then reconstructed from the boundary data. The ability to detect spatial locations and magnitudes of multiple damages has been demonstrated with a sensitivity of 73 ppm in sensing area. In addition, we have assessed the detection limit of CNCP sensor by ERT and the experimental results show the limit as 29 ppm in sensing area, which is at least 30 times better than previous results in the literature. The small thickness of the paper substrate and high conductivity of the SWCNTs enable the observed sensitive detection of damages.

MATERIALS AND METHODS

Carbon Nanotube Coated Filter Paper (CNCP). A total of 50 mg of single-walled carbon nanotubes (SWCNTs) (Nano Amor) and 100 mg of SDBS (sodium dodecylbenezene sulfonate, Sigma-Aldrich) were dispersed in 10 mL of deionized water.[17,19] After bath sonication (Branson) for 10 min, the SWCNT dispersion was probe-sonicated for 2 h at 25 W (Misonix, XL-2000). The color of the solution was getting darker with increased sonication. A thin plastic tape was attached to the bottom of the filter paper to enhance physical durability during any solution deposition (Figure 1a, right). Dispersed SWCNT solution was deposited on the filter paper ($d = 7$ cm) using a paintbrush (Figure 1a, left) and the samples were then air-dried. Deposition and drying were repeated several times to reduce the resistance. Overall, an extra coat can reduce the resistance to half the original value (see Table S1 under Supporting Information).

Three samples with different resistance values (A, B, and C) and one duplicate sample (A′) were prepared. The resistance uniformity over the sample and the base resistance were monitored and adjusted carefully by multiple depositions of SWCNT solution with the paintbrush. The resistance between two adjacent electrodes were measured and analyzed statistically to evaluate the sample uniformity before any damage experiments (Table S1, Supporting Information). The CNCPs show lower or comparable RSD (relative standard deviation, %) compared to other commercially available thick panel samples (for example, ABS/PVC or glassy carbon) and visually tighter resistance distribution over 16 electrodes (see Figure S1 under Supporting Information).

Measurement System. For ERT measurement, the current needs to be injected into one electrode when another electrode is set to ground and the remaining two electrodes are to set to measure the voltage. The measurement system consists of a DC source (Keithley 6430) and a switching unit with an internal digital multimeter (Keithley 2701). The DC source delivers from 2.5 to 20 mA current to the ERT sample. The input current, depending on the sample resistance, was limited by the digital multimeter which is only able to measure up to 21 V.

ERT Measurement Scheme. Adjacent method was used for signal stimulation and voltage measurements. This method is more sensitive to variations in the resistance of damages near the electrodes than in the center of the CNCP. Voltage measurements involving the injecting or grounded electrodes were not included in measurements. Thus, the current simulating started from electrode 1−2 pair (Figure 1b, 1 in red colored) and the voltage was measured from successive electrode pairs such as 3−4, 4−5, ..., 15−16, giving 13 voltage measurements. Voltages across electrode pair, 1−2, 2−3, and 16−1 were skipped since the current was injected from electrode 1−2 pair. Then the second set of measurements was made with the current applied at electrode 2−3 pair, giving a further 13 sets of voltage data. This process was repeated generating a total of $16 \times 13 = 208$ voltage measurements. All the 208 data were used for the image reconstruction.

Image Reconstruction and Statistical analysis. Images were reconstructed using EIDORS (Electrical Resistance and Diffuse Optical tomography Reconstruction Software) package,[23,24] and this software package consists of four primary objects: forward model, inverse model, data, and image. A finite element model is used to solve the forward model in EIDORS. The inverse model was performed using differential image reconstruction using two data objects. One set was from the background with no damage and the other set from the measurements with intentional damages. For statistical evaluation of reconstructed images, NaN-Tb statistics toolbox was used.

Conflict of Interest: The authors declare no competing financial interest.

Acknowledgment. This work was supported by the Nanotechnology Thematic Project in NASA's Game Changing Development Program.

Supporting Information Available: Base resistances and damage responses of various CNCPs, ERT simulations to determine hyperparameter and detection limit, and ERT simulations for moving damages. This material is available free of charge *via* the Internet at http://pubs.acs.org.

REFERENCES AND NOTES

1. Loh, K. J.; Hou, T. C.; Lynch, J. P.; Kotov, N. A. Carbon Nanotube Sensing Skins for Spatial Strain and Impact Damage Identification. *J. Nondestruc. Eval.* **2009**, *28*, 9–25.
2. Ross, R. W.; Hilton, Y. L. Damage Diagnosis in Semiconductive Materials Using Electrical Impedance Measurements. 49th AIAA/ASME/ASCE/AHS/ASC Structures, Structural Dynamics and Materials Conference, Schaumburg, IL, April 7−10, **2008**; p 1936.
3. Borcea, L. Electrical Impedance Tomography. *Inverse Probl.* **2002**, *18*, R99–R136.
4. Baltopolos, A.; Polydorides, N.; Pambaguian, L.; Vavoulitotis, A.; Kostopoulos, V. Damage Identification in Carbon Fiber Reinforced Polymer Plates using Electrical Resistance Tomography Mapping. *J. Compos. Mater.* **2013**, *47*, 3285–3301.
5. Hou, T. C.; Loh, K. J.; Lynch, J. P. Spatial Conductivity Mapping of Carbon Nanotube Composite Thin Films by Electrical Impedance Tomography for Sensing Applications. *Nanotechnology* **2007**, *18*, 315501.
6. Loh, K. J.; Kim, J. H.; Lynch, J. P.; Nadine, W. S. K.; Kotov, N. A. Multifunctional Layer-by-layer Carbon Nanotube-polyelectrolyte Thin Films for Strain and Corrosion Sensing. *Smart Mater. Struc.* **2007**, *16*, 429–438.
7. Vadlamani, V. K.; Chalivendra, V.; Shukla, A.; Yang, S. *In Situ* Sensing of Non-linear Deformation and Damage in Epoxy Particulate Compsites. *Smart Mater. Struct.* **2012**, *21*, 075011.
8. Hu, N.; Karube, Y.; Yan, C.; Masuda, Z.; Fukunaga, H. Tunneling Effect in a Polymer/Carbon Nanotube Nanocomposite Strain Sensor. *Acta Mater.* **2008**, *56*, 2929–2936.
9. Gao, L.; Chou, T. W.; Thostenson, E. T.; Zhang, Z.; Coulaud, M. *In Situ* Sensing of Impact Damage in Epoxy/Glass Fiber Composites Using Percolating Carbon Nanotube Networks. *Carbon* **2011**, *49*, 3382–5.
10. Thostenson, E. T.; Chou, T. W. Real Time *in Situ* Sensing of Damage Evolution in Advanced Fiber Composites using Carbon Nanotube Networks. *Nanotechnology* **2008**, *19*, 215713.
11. Saffi, M. Wireless and Embedded Carbon Nanotube Networks for Damage Detection in Concrete Structures. *Nanotechnology* **2009**, *20*, 395502.
12. Todoroki, A.; Tanaka, M.; Shimamura, Y. High Performance Estimation of Delamination of Graphite/Epoxy Laminates with Electric Resistance Change Method. *Compos. Sci. Technol.* **2003**, *63*, 1911–1920.
13. Todoroki, A.; Tanaka, M.; Shimamura, Y. Multi-probe Electric Potential Change Method for Delamination Monitoring of Graphite/Epoxy Composite Plates using Normalized Response Surface. *Compos. Sci. Technol.* **2004**, *64*, 749–758.
14. Han, J. W.; Kim, B.; Li, J.; Meyyappan, M. Carbon Nanotube Based Humidity Sensor on Cellulose Paper. *J. Phys. Chem. C* **2012**, *116*, 22094–22097.
15. Han, J. W.; Kim, B.; Li, J.; Meyyappan, M. A Carbon Nanotube Based Ammonia Sensor on Cellulose Paper. *RSC Adv.* **2014**, *4*, 549–553.
16. Ammu, S.; Dua, V.; Agnihotra, S. R.; Surwade, S. P.; Phulgirkar, A.; Patel, S.; Manohar, S. K. Flexible All-organic Chemiresistor for Detecting Chemically Aggressive Vapors. *J. Am. Chem. Soc.* **2014**, *134*, 4553–4556.
17. Hu, L.; Choi, J. W.; Yang, Y.; Jeong, S.; Mantia, F. L.; Cui, L. F.; Cui, Y. Highly Conductive Paper for Energy-Storage Devices. *Proc. Natl. Acad. Sci. U.S.A.* **2009**, 21490–21494.
18. Han, J. W.; Kim, B.; Li, J.; Meyyappan, M. Carbon Nanotube Ink for Writing on Cellulose Paper. *Mater. Res. Bull.* **2014**, *50*, 249–253.
19. Islam, M. F.; Rojas, E.; Bergey, D. M.; Johnson, A. T.; Yodh, A. G. High Weight Fraction Surfactant Solubilization of Single-wall Carbon Nanotubes in Water. *Nano Lett.* **2013**, *3*, 269–273.
20. Sun, T.; Tsuda, S.; Zauner, K. P.; Morgan, H. On-chip Electrical Impedance Tomography for Imaging Biological Cells. *Biosens. Bioelectronics* **2010**, *25*, 1109–1115.
21. Loyola, B. R.; Saponara, V. L.; Loh, K. J.; Briggs, T. M.; O'Bryan, G.; Skinner, J. L. Spatial Sensing Using Electrical Impedance Tomography. *IEEE Sensors J.* **2013**, *13*, 2357–2367.
22. Polydorides, N.; Lionheart, W.R. B. Matlab Toolkit for Three-dimensional Electrical Impedance Tomography: A Contribution to the Electrical Impedance and Diffuse Optical Reconstruction Software Project. *Meas. Sci. Technol.* **2002**, *13*, 1871–1883.
23. Adler, A.; Lionheart, W. R. B. Uses and Abuses of EIDORS: An Extensible Software Base for EIT. *Physiol. Meas* **2006**, *27*, S25–S42.
24. Currie, L. A. Nomenclature in Evaluation of Analytical Methods including Detection and Quantification Capabilities. *Pure Appl. Chem.* **1995**, *67*, 1699.